

Performance modeling of unmanaged hybrid battery/supercapacitor energy storage systems

Mohammed Ahmed Zabara, Can Berk Uzundal¹, Burak Ülgüt^{*}

Department of Chemistry, Bilkent University, Ankara, Turkey

ARTICLE INFO

Keywords:

Hybrid Battery/Supercapacitor Systems
Parallel Connection
Current Distribution
Current Profiles
Electrochemical Impedance Spectroscopy

ABSTRACT

Unmanaged hybrid battery/supercapacitor energy storage systems possess higher performance with lower cost and complexity compared to not only individual cells, but also electronically managed hybrid systems. Achieving full performance requires the understanding of the power distribution and predicting their best combinations. In this work, a semi-empirical modeling methodology is presented that can predict the current distribution and the voltage response of battery/supercapacitor hybrid systems under arbitrary charge/discharge profiles. Results are presented for the assessment of hybrid systems under real life scenarios. The key strength of the presented method is that it is free of any parametrization, fits or subjective inputs. The modeling methodology is validated with experimental measurements for two different Li-ion battery chemistries, namely Lithium Iron Phosphate and Lithium Vanadium Pentoxide, connected in parallel to wide range of supercapacitors. Finally, we outline several design rules for hybrid storage systems for different use cases.

1. Introduction

High-performance electrochemical energy storage systems which can store large amount of energy (high-energy-density) and charge/discharge rapidly (high-power-density) are in great demand [1,2]. Lithium-ion (Li-ion) batteries are considered the state-of-the-art electrochemical energy storage devices used widely in transportation, electronics and stationary applications. However, due to limitations of the underlying electrochemical properties, they suffer from capacity degradation and reduced cycle life if used under high power density conditions [2,3]. Supercapacitors on the other hand, possess high power density with 10-times larger cycle life than Li-ion batteries. However, their energy density is low and are much smaller than Li-ion batteries [4,5].

To obtain high energy together with high power densities, hybridization of Li-ion batteries with supercapacitor through parallel connection has been proposed in the literature [6,7]. Hybridization offers the advantages of both devices and mitigates the negative effects of quick changes or high levels of charge and/or discharge of the high-power-density applications [8–10]. The parallel connection of Li-ion battery to a supercapacitor allows the current to be distributed

among both devices and the voltage on the terminals to be equal [6].

In the literature, aiming for an increase in battery/supercapacitor performance, various studies proposed the use of converters and control circuits to manage the current distribution among the components of the hybrid systems [11–14]. This severely limits the application for not only the reason of added cost, but also due to the reduction in reliability and durability [8]. Unmanaged hybrid systems are the better configuration of hybridization for maximized performance tailor-made for given use cases. Achieving their full performance requires understanding of the power distribution under various conditions and combinations. This requires an accurate performance modeling methodology which can assess their performance in realistic scenarios and predict the best combination of batteries and supercapacitor tailored to the application.

Typically, energy storage systems are assessed through power and energy density comparisons measured under constant current² which are good for standardization but not practical for realistic estimations [15–17]. Different applications require assessing the performance during tailored charge and discharge sequences of varying depths and rates. Proper analysis involves much more than a capacity comparison for hybrid systems, since the details of cell resistance and capacitance play a huge role in how the system behaves under arbitrary charge/discharge

^{*} Corresponding author.

E-mail address: ulgut@fen.bilkent.edu.tr (B. Ülgüt).

¹ Present Address: Department of Chemistry, University of California, Berkeley, California 94720, USA.

² Ragone plots, which are a standard way of visualizing energy and power densities measured under constant current, are routinely employed

scenarios [18–20]. For example, in the automotive industry, a typical automobile performance has to be simulated for well above a couple hundred drive cycles in the design phase [21]. This undoubtedly includes the simulation of the energy storage system.

In the literature, the performance of unmanaged hybrid systems was simulated by means of equivalent circuit models where a combination of voltage source, resistors, and capacitors are used for the simulation [6,8,15]. In these studies, Ragone plots were implemented to evaluate their performance under pulse discharge current. As another approach, Sikha et al. presented a one-dimensional mathematical model for the simulation of Li-ion and 10F system under pulse current profile [22]. The study also used Ragone plots for the comparison of the energy densities of the systems before and after the hybridization. However, the presented modeling studies did not provide a comparison for hybrid systems under real life scenarios with application oriented current profiles. Moreover, the equivalent circuit models are dependent on the subjective inputs in its parameter determination [23,24]. The strength of any modeling method relies on its good agreement with the experimental measurement and in minimizing the number of free parameters. Therefore, there is a need for a modeling methodology that can accurately predict the performance of battery/supercapacitor hybrid systems under real life scenarios and employs objective approaches that don't require human interpretation.

In this work, we introduce a semi-empirical modeling methodology which can predict the current distribution and the voltage response of arbitrarily chosen hybrid systems under arbitrary charge/discharge profiles. We present the results of our method validated with experimental measurements for assessment of two different Li-ion battery/supercapacitor hybrid systems under real life scenarios. We further show optimization parameters for predicting the best combinations for the demanded attributes in given applications. The key strength of this method is that it is free of any parametrization, fits or subjective inputs. With two measured inputs, namely the impedance spectrum and equilibrium charge/voltage lookup table employed directly, current distribution and the voltage of the hybrid system are calculated under arbitrary current profiles. Lithium Iron Phosphate (LFP) and Lithium Vanadium Pentoxide (LVO) batteries were hybridized with different supercapacitors ranging from 10mF to 500F. The simulated results showed good agreement with the experimental measurements with proportional errors of less than 1% in most cases.

2. Modeling algorithm

To obtain the current distribution and the voltage response of a battery/supercapacitor hybrid system, we employed an extension of our previously published algorithm [18]. The algorithm was able to accurately model the voltage response of single cells of primary and secondary batteries as well as supercapacitors [18,25,26]. In the current work, to accurately model current distributions across hybrid systems, a Differential Evolution (DE) algorithm is incorporated to iteratively optimize the current distribution for hybrid systems. DE is chosen because of its ability to solve non-differentiable functions by its stochastic direct search and its convergence properties [27].

2.1. Differential evolution algorithm for current distribution optimization

The DE routine finds the optimal current across each energy storage device under two constraints. The first is, as hybrid storage devices are connected in parallel, the sum of currents across the individual arms needs to be equal to the total current passing through the stack. The total current is the current applied to the hybrid system for the tailored application. The second is, the voltages of the individual arms are always required to be equal. The voltage here is calculated utilizing the electrochemical impedance of the components which is explained in zero-free-parameter voltage calculation section.

DE utilizes D-dimensional parameter vectors as a population of

individuals for each generation. In our case, the components of the vectors are the currents passing through each component I_{battery} and $I_{\text{supercapacitor}}$.

The two constraints are implemented as follows:

For the current restraint, the current through the supercapacitor is defined as the total current minus the current through the battery at every point. This decreases the number of parameters to be optimized, while also maintaining the constraint.

$$I_{\text{supercapacitor}}[t] = I_{\text{total}}[t] - I_{\text{battery}}[t] \quad (1)$$

- The voltage constraint is used as the cost function to be minimized. That is:

$$\text{Cost Function} = \sum_t |E_{\text{battery}}[t] - E_{\text{supercapacitor}}[t]| \quad (2)$$

The details for the DE method are summarized in supplementary materials (SM1).

2.2. Zero-free-parameter voltage calculation

To obtain the voltage response of the hybrid components, zero-free-parameter method is used which provided accurate results for single cells [18]. The main computation is in obtaining the voltage of each hybrid device at the frequency domain based on Ohm's law using the Electrochemical Impedance Spectroscopy (EIS) data:

$$E'_i(f) = I_i(f) \times Z_i(f) \quad (3)$$

Where $Z_i(f)$ is the impedance of the device (i), which can be a battery or a supercapacitor, obtained from the EIS measurement at the corresponding frequencies and $I_i(f)$ is the current values of the applied current profile in the frequency domain obtained from the Fourier transform of the chosen current profile for specific application:

$$I(t) \Rightarrow^{FFT} I(f) \quad (4)$$

The calculated voltage response is then converted from the frequency domain to the time domain using inverse Fourier transform:

$$E'_i(f) \Rightarrow^{iFFT} E'_i(t) \quad (5)$$

The final step is to add the equilibrium charge/voltage values $E_i(Q)$ which are obtained from look up tables collected for each system. The final result is the voltage at the State-of-Charge of the component:

$$E'_i(t) + E_i(Q) = E_i(t) \quad (6)$$

This method is used to calculate the total voltage of the hybrid system which is used for predicting the current distribution among the hybrid components. There exists a difference between the total measured voltage of the measurement set-up and the terminal voltage of the components. This difference is related to the stray resistance which is the resistance of the current at paths of the measurement set-up. To compensate for this voltage difference, we have measured the EIS of each component at the terminals and while connected to the measurement set-up which included the stray resistance. For calculation of the total voltage of the hybrid system, the EIS data of the component with the stray resistances were used.

2.3. Current profiles

Three current profiles were chosen to test the modeling method with three distinct charge/discharge scenarios. The first scenario is a slow charge/discharge which is named as profile-1. The profile demonstrates the slow response to current depths of fixed time periods. The slow profile is specifically picked to test our methodology since long plateaus

are the toughest for our algorithm [25]. The second scenario is a fast-fluctuating profile demonstrating the fast response of the system at various current depths which is named as profile-2. This profile was obtained from Worldwide Harmonized Light Vehicle duty cycle published by United Nations Economic Commission for Europe [28]. The third scenario is a charge/discharge square wave which was used to study the symmetric response of the hybrid systems while further straining our algorithm. The three profiles are shown in Fig. 2. For LFP/Supercapacitor systems the current amplitude was adjusted to range between 0.5C to 2C for profile-1 and maximum of 1C for profile-2. For LVO/Capacitor systems the maximum current was adjusted not to exceed 1.5C for both profiles.

3. Experimental

3.1. Batteries and supercapacitors

Modeling methodology was tested for two hybrid systems with two Li-ion chemistries and wide range of supercapacitors. The systems and their parameters are as follow:

LFP/Supercapacitor - Lithium Iron Phosphate (LFP) 18650 size battery with 1500mAh capacity and 3.2 V nominal voltage was used at 100% State-of-Charge. The cell was connected to supercapacitor with 1, 10, 25, 100 and 400F. The maximum voltage of the supercapacitor was 2.7V which is lower than the voltage of the LFP. To increase the voltage of the supercapacitor, we connected two identical supercapacitors in series which resulted in increasing the maximum voltage to 5.2V. However, the series connection resulted in decreasing the capacitance of the identical supercapacitor to half. As a result, LFP/0.5, 5, 12, 50, 200F systems were studied.

LVO/Capacitor - Lithium Vanadium Pentoxide (LVO) coin battery with 20mAh capacity and 3.0 V nominal voltage at 100% State-of-Charge. LVO cell was connected to capacitors with 10mF and 20mF capacitance. The maximum voltage of these capacitors was 6.3V.

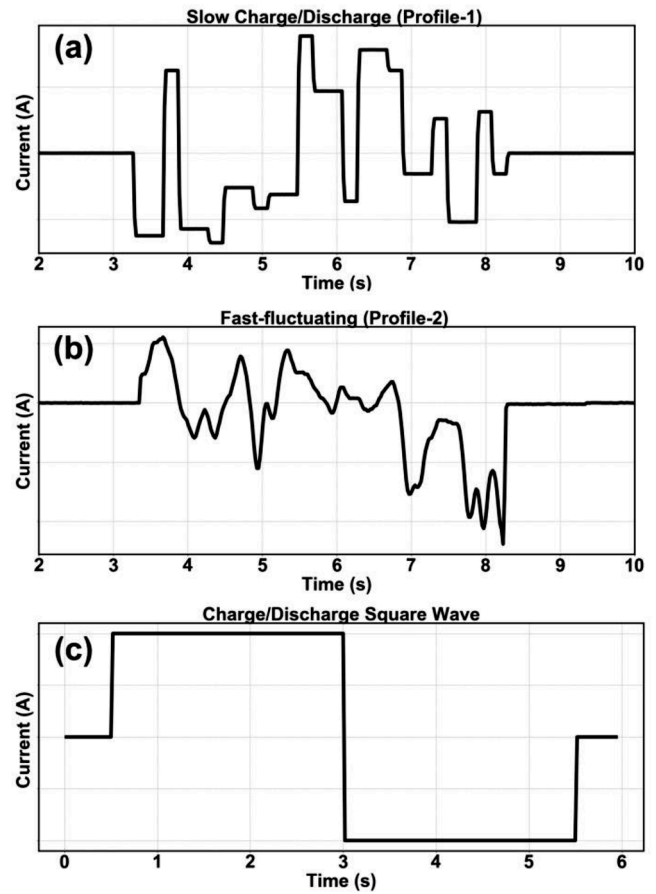


Fig. 2. Current profiles applied to study the performance of the hybrid systems (a) Slow charge/discharge (Profile-1), (b) Fast-fluctuating (Profile-2), (c) Charge/discharge square wave

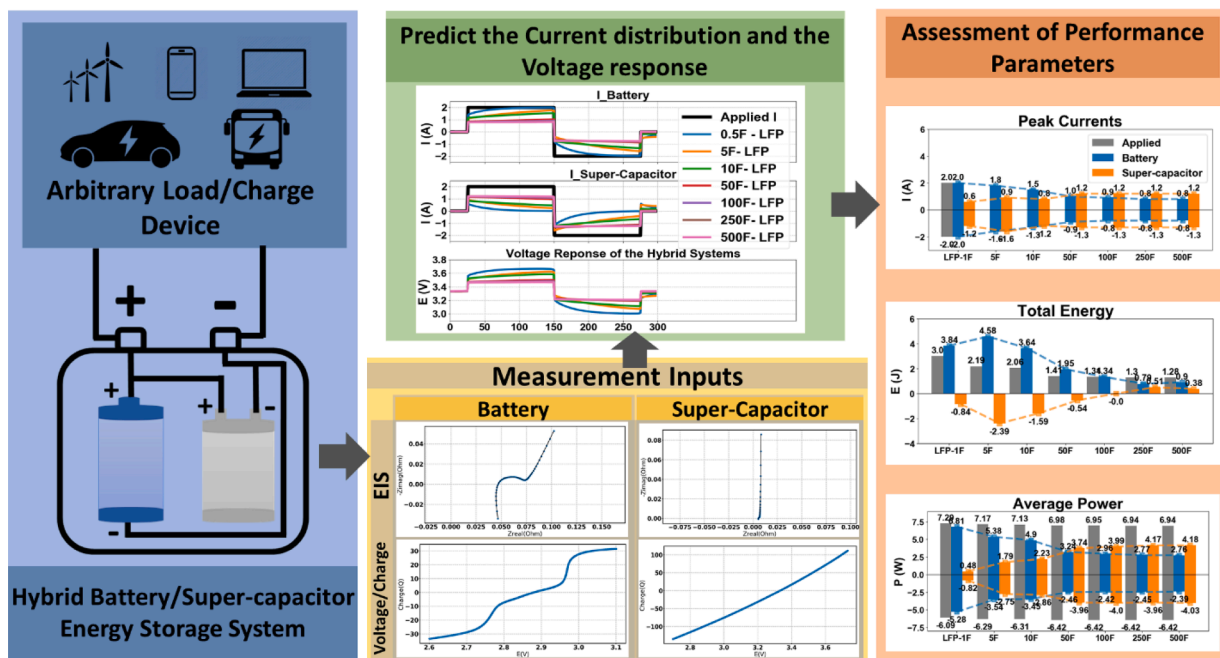


Fig. 1. An overview of the performance modeling methodology of battery/supercapacitor hybrid system under arbitrary load/charge profile. First the current distribution and the voltage response are predicted from Electrochemical Impedance spectrum and equilibrium charge/voltage lookup tables then performance parameters are obtained to determine the best combination of battery/supercapacitor hybrid system

3.2. Electrochemical measurements

3.2.1. Electrochemical impedance spectroscopy

EIS data of the batteries and the supercapacitors were obtained in potentiostatic mode using Gamry Interface 5000. The measurement script was adjusted to obtain the linearly spaced EIS spectra with the user defined parameters. In a typical measurement, excitation amplitudes of 5mV were applied between 50 and 0.2 Hz with 0.2 Hz sampling. EIS data are shown in supplementary materials (SM2).

3.2.2. EIS simulations

EIS data was simulated for supercapacitors with capacitance ranging from 1F to 500F using a transmission line model (Bisquert Open) [29]. For a given intended capacitance, the transmission line model had two input parameters which are, the solution resistance R_u , and the series pore resistance R_m . The EIS data of 1, 10, 25, 100 and 400F supercapacitors were used to parametrize the transmission line model. This parametrized model was used to determine the appropriate values of R_u and R_m for the EIS simulations. The Transmission Line model and the fitted parameters are shown in supplementary materials (SM3).

3.2.3. Charge/voltage maps

The voltage behavior vs. charge maps were obtained by charging each device at low currents. LFP was charged with 1mA from 2.8 to 3.8V. LVO was charged with 500 μ A from 2.4 to 3.4V. Supercapacitors with capacitance from 0.5 to 200F were charged with 1mA and with capacitances between 10mF to 100mF by 100 μ A.

The charge/voltage map for simulated supercapacitors was calculated using:

$$V = \frac{Q}{C} \quad (7)$$

Where V is the supercapacitor's potential in Volts, Q is the charge in Coulomb and C is the capacitance in Farads. The voltage of the supercapacitor at $Q = 0$ was assigned to the Open Circuit Potential of the hybrid system which correspond to the zero current in the applied current profiles.

3.3. Measurement set-up

To validate the predicted current distribution and voltage response obtained by the modeling method, we constructed a measurement set-up. The setup can simultaneously measure the individual currents passing over the hybrid devices and the voltage at their terminals. The current measurements were done using Hall effect transducers to circumvent the added impedance of shunt resistors. Given the resistance of an energy storage device (\sim m Ω), the added shunt resistance in series to an energy storage device would dominate the measured response. Further, as the current levels investigated approaches greater than 1 A, the resistance of the shunt resistor is liable to thermal drifts. The circuit for the current measurement is provided in supplementary materials (SM4). The voltages from the current sensors and the voltages at the terminals of the hybrid components were measured using a DAC (NI USB-6229). The DAC was controlled with Python 3.5 using the NI-DAQmx package under Scientific Python Developing Environment (Spyder 2.3.5.2) [30,31]. The current profiles were applied to the hybrid systems connected to the measurement set-up by Gamry Interface 5000. An in-house written script was used to apply the current values of the intended profiles at the specifies sampling rate. The details regarding the data acquisition system are provided in supplementary materials (SM4).

4. Results and discussion

The developed method was first validated with experimental measurements for two Li-ion battery/Supercapacitor systems under profile-1 and profile-2. For these systems the EIS and charge/voltage

measurement inputs were obtained experimentally. Here, we will first show the accuracy of the modeling method compared to experimental measurements. Then results from simulated supercapacitor systems are shown followed by our suggestions for optimal performance under various use-cases for the hybrid devices.

4.1. Hybrid LFP-supercapacitor systems

In Fig. 3, the overlay of simulated and experimentally measured current distribution and voltage responses of hybrid LFP/supercapacitor with 0.5F and 200F systems are shown. The proportional error plots are provided in supplementary materials (Fig. SM7). Simulations for different systems are also shown in supplementary materials (Fig. SM6). As can be seen, the simulations and the experimentally measured data agree within 2% in all cases and 1% in majority of the cases. The agreement between the experimentally measured and the simulated results in both profiles demonstrates the high accuracy of the method to predict the current distribution and to determine the voltage response of the LFP/supercapacitor systems.

4.2. Hybrid LVO-capacitor systems

The method was also successful in predicting the current distribution and the voltage response of small capacity hybrid systems but with higher proportional percent error. In Fig. 4, the overlay of simulated and experimentally measured results of parallel-connected Lithium Vanadium Pentoxide (LVO) battery and two capacitors (10mF, 20mF) are shown. The percent proportional errors are shown in Fig. SM8 in supplementary material. The raise in the percent error is due to the decrease in the device's capacity and the amplitudes of the current applied [32].

4.3. Hybrid battery/supercapacitor systems with simulated EIS for supercapacitors

Having demonstrated the high accuracy of the developed methodology, we set out to investigate simulated hybrid systems. In Fig. 5(a) simulations for square wave profile for LFP and simulated supercapacitors hybrid systems are shown. The simple square wave profile helps in visualizing the effect of capacitance on the current distribution and the voltage response of LFP/supercapacitor hybrid systems. For the charging pulse, the current is passing heavily through the LFP when hybridized with 5 and 10 F. The charging pulse is almost shared equally at 50F and then is mostly passing through 100 and 500F. In all systems the take-off current is shared by both LFP and the supercapacitors. Progressing through the pulse, the current passing through the supercapacitor arm decreases at 5 and 10F while the current passing through the LFP increases. This is due to the low capacity of 5 and 10F supercapacitors at this current level. When hybridized with higher capacitances (50, 100 and 500F), the take-off current favors the supercapacitor. The current over the supercapacitor arm also remains higher than the LFP arm. The current over the supercapacitors decrease over time for 50 and 100F but is almost constant for 500F. The above observations are consistent with the increase in the capacitance of the supercapacitors. It is important to note that although there is a large increase in the capacitance going from 100 to 500F there is no big increase in the current passing through the supercapacitor. In this case the current is limited by the impedance of the supercapacitors and the stray resistance.

The discharge pulse is applied directly after the charging pulse. At the current jump, from 2A to -2A, the current is mostly drawn from the supercapacitors. The current over the supercapacitors then decreases for 5 and 10F and is overtaken by the LFP while the current over the supercapacitor remains higher for 50, 100 and 500F at all times. After the pulse, although the total current is zero, the LFP charges the 5 and 10F supercapacitors to reach equilibrium which is not observed for higher capacitances 100 and 500F.

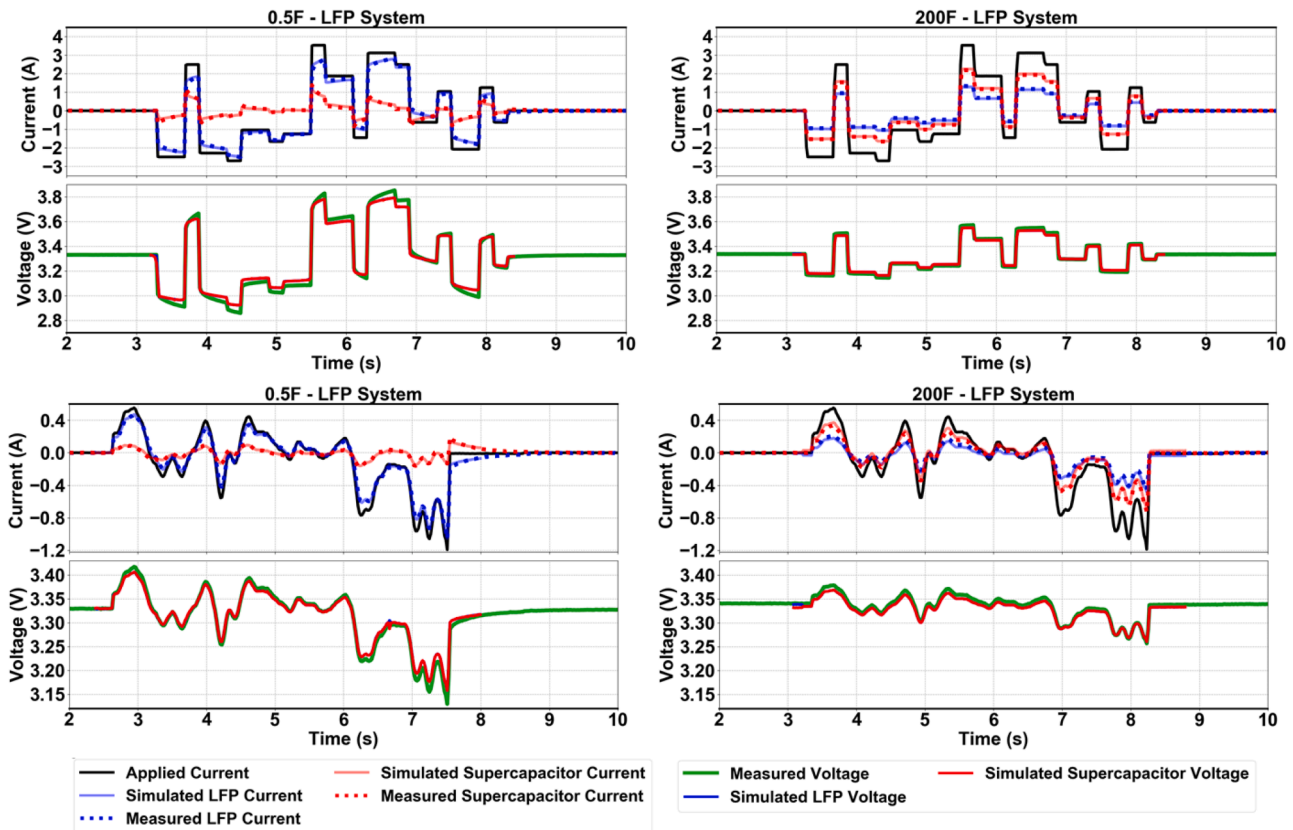


Fig. 3. Overlays of simulated and experimentally measured current distributions and voltage responses for parallel-connected Lithium Iron Phosphate (LFP) battery and supercapacitors of 0.5F and 200F under profile-1 (top) and profile-2 (bottom). In the current response, black lines represent the total applied current, blue lines are the current passing through the LFP and the red lines are for the supercapacitor. Voltage response shows the measured voltage in green lines and the simulated voltage in red and blue lines resulting from the applied current profile.

The voltage response of the system displays a decrease in the pulse amplitudes as the capacitance increases. This is related to the decrease in impedance as the capacitance increases. The shape of the voltage response to the current pulse also varies where it shows an increase in voltage at charge and a decrease at discharge for 5, 10 and 50F and almost stays at constant voltage for higher capacitances.

4.4. Performance parameters

The performance of the hybrid system varies with changing the capacitance. To facilitate the assessment of their performance, we assigned performance parameters which provide information to best combine and optimize the hybrid systems. We define the metrics to be used to evaluate the hybrid systems as follows:

- **Peak Current** is the maximum current that passes through the battery and the supercapacitor.
- **Average Power Distribution** defined as the sum of the power through the applied current profile divided by the number of sampling points.

$$\hat{p} = \frac{\sum_{i=1}^n P_i}{n} \quad (8)$$

where $P_i = E_i \times I_i$ (9)

- **Total Charge Distribution** defined as the sum of the charges obtained from the integration of the current distribution through time.

$$Q_T = \int_0^t I(t)dt \quad (10)$$

- **Total Energy** obtained from the integration of the total power through the time of the current profile applied.

$$E_T = \int_0^t P(t)dt \quad (11)$$

The trends in these metrics vs. the capacitance can be used to understand the systems performance. These trends can also be used to find tailored hybrid systems for various use cases (as demonstrated by their unique current profiles). Fig. 5 (b) shows the extracted performance metrics for LFP/Supercapacitor (5,10, 50, 100 and 500F) hybrid systems under the square wave profile shown in Fig. 6(a). The trends are as follows:

Peak Current _ Although the pulse was applied for 2.5 seconds, we can assign the peak current as the maximum point reached by the current of each system. Taking this into consideration, we can see that the peak current decreases for the LFP and increases for the supercapacitor from 5 to 50F. It then remains constant with increasing the capacitance. This is related to the stray impedance of the hybrid system.

Average Power Distribution and Total Charge Distribution _ Evaluating the total charge and the average power provides clearer trends as the capacitance increases. The charge and the average power distribution increase for the supercapacitor matched with a decrease in the LFP by increasing the capacitance. However, the increase is non-linear in which it flattens after 50F.

Total Energy _ The total energy distribution shows the sum of the energy from the two pulses. It shows positive values when any component charges and negative if it discharges. The total energy shows positive values for the LFP with a decreasing value as the capacitance

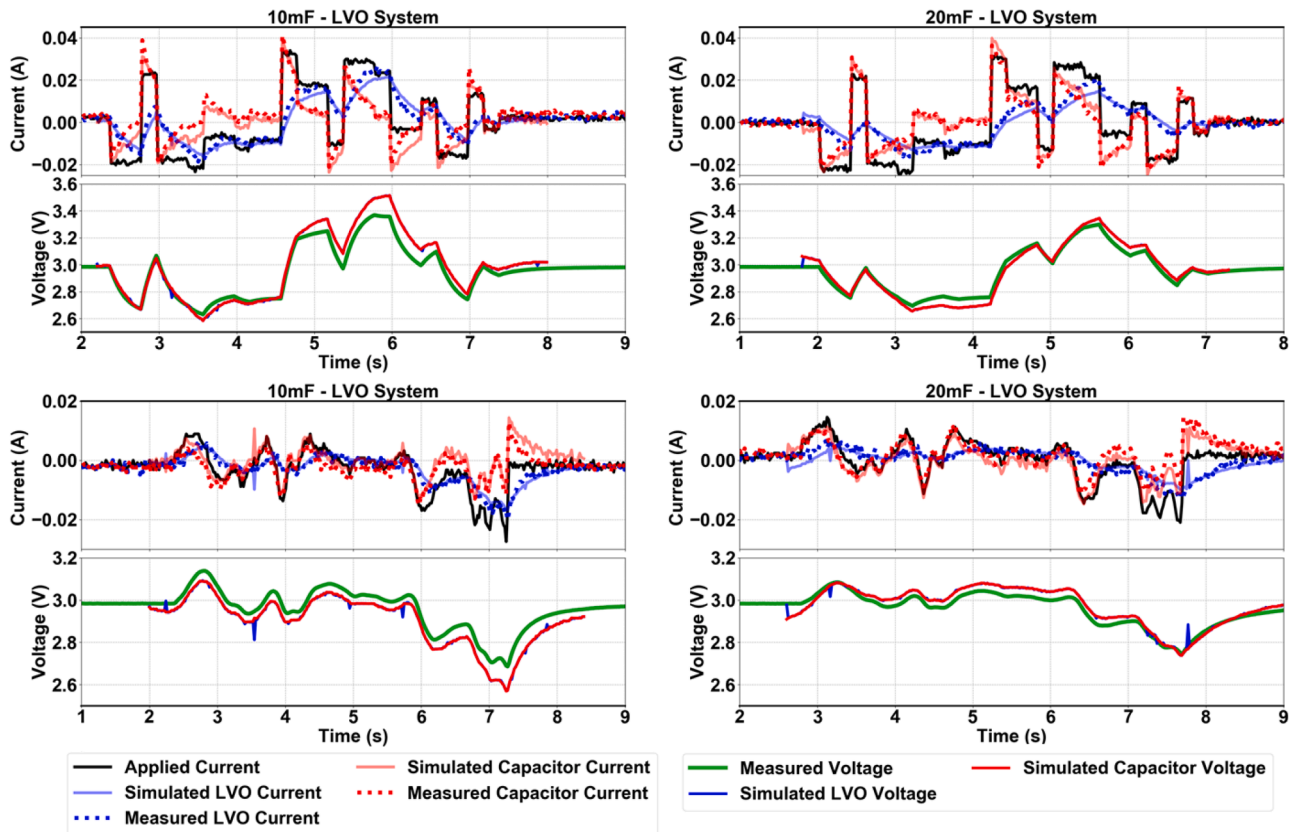


Fig. 4. Overlays of simulated and experimentally measured current distribution and voltage response of Lithium Vanadium Pentoxide (LVO) battery and 10mF and 20mF capacitors under current profile-1(top) and profile-2(bottom).

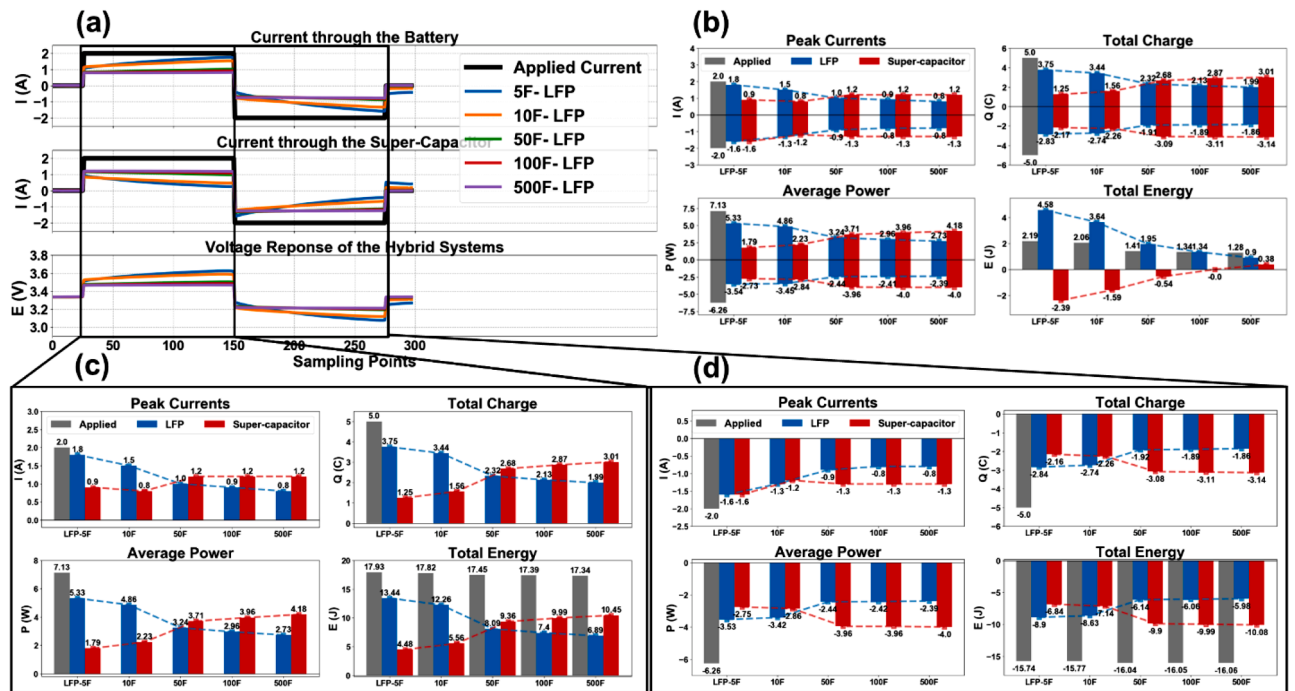


Fig. 5. (a) Simulated current distribution and the voltage response of LFP and simulated supercapacitor (5F, 10F, 50F, 100F and 500F) hybrid system under a square wave profile of 2A followed by -2A current pulses. Performance parameters: Peak Current, Total Charge, Average Power, and Total Energy for the simulated systems under (b) Total square wave profile, (c) Charging pulse, (d) Discharge pulse.

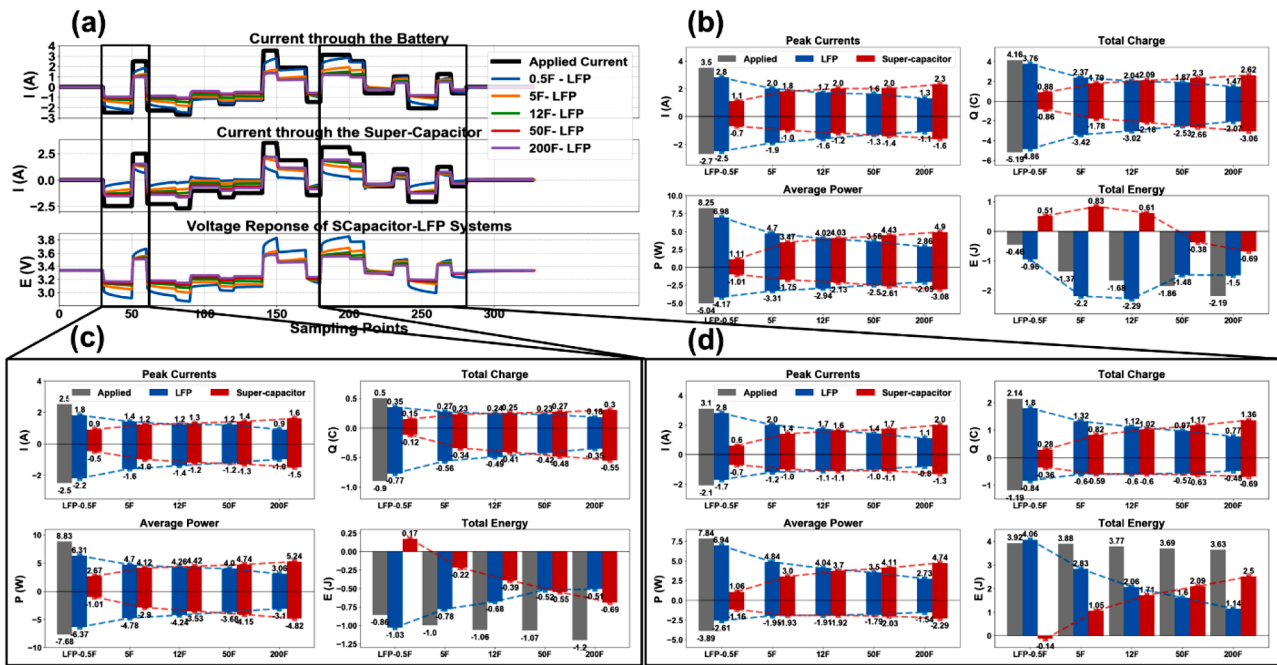


Fig. 6. (a) Current profile-1, Performance parameters: Peak Current, Total Charge, Average Power, and Total Energy for different LFP-0.5, 5, 12, 50 and 200F systems for (b) All the profile, (c) First region, (d) Second region

increases. In the case of the supercapacitors, it discharges at 5, 10 and 50F with decrease in the total energy and charges at 500F with zero total energy at 100F.

Performance parameters are also analyzed separately for the charge and the discharge pulse shown in Fig. 5(c and d). Benefits of unmanaged hybridization in providing rapid response and protecting the battery at such fast changes is observed at the discharged pulse where the current jump from 2A to -2A is taking place. Supercapacitor is clearly acting as a buffer and protects the battery from the fast change in the current. In the charging pulse both the battery and the supercapacitor almost share the charge, power and energy equally at around 50F but at the discharge

pulse, due to the fast change, supercapacitor is more effective even at lower capacitances.

The analysis is done for the other profiles which represent real life scenario applications with the profiles shown previously for profile-1 and 2. In Fig. 6 and 7. we show examples of parameter analyses for the entire profiles and from specific regions. Parameters calculated using the entire profile show complex trends due to the summation over various current depths and rates. However, analysis of sub-regions provides intuitive trends to understand the behavior of the systems.

Peak Current - Peak current passing through the LFP decreased by increasing capacitance of the parallel connected supercapacitor. The

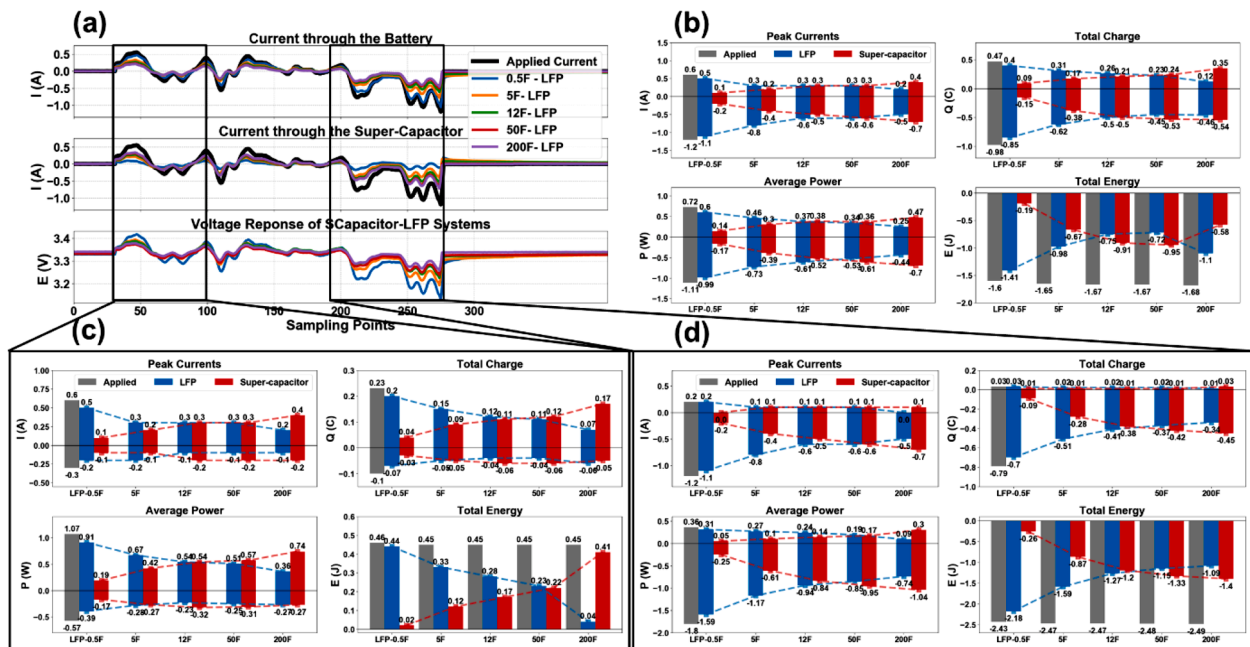


Fig. 7. (a) current profile-2, Performance parameters: Peak Current, Total Charge, Average Power, and Total Energy for different LFP-0.5, 5, 12, 50 and 200F systems for (b) All the profile, (c) First region, (d) Second region

lower peak current is preferred for batteries. A hybrid system with a large enough supercapacitor is expected to result in a longer cycle life for the battery by avoiding Li plating [33,34]. For instance, in applications where batteries encounter bursts of current for short durations, a 10F or higher supercapacitor in parallel to the LFP is predicted to be beneficial for cycle life. The extended cycle life would serve to benefit applications such as GSM and other portable electronics. However, the rate of peak current decrease is not linear. The decrease is high moving from 0.5F to 10F which is around 600mA, but the effect is lowered moving to higher capacitances. It only decreases by 300mA moving from 10F to 200F.

Average Power Distribution – The power distribution is almost following a linear trend with increasing the capacitance in which the power is heavily supplied by the battery for the low capacitances and heavily by the supercapacitor in the high capacitances. The power is equally shared for the capacitance value between 12F and 50F in both profiles.

Total Energy and Charge Distribution – Comparing the energy and charge distribution, more charge and energy is shared by the supercapacitor by increasing the capacitance. It is observed that almost equal distribution is obtained for LFP-50F hybrid system. In the case of LFP-0.5F system, although the applied current pulse results in negative total energy for the region shown in Fig. 7 (c), the 0.5F capacitor shows positive energy distribution. This shows that the capacitor is causing extra load on the LFP resulting in faster discharge of the LFP which should be avoided.

Evaluation of performance under the employed current profiles exhibits the advantages of the battery/supercapacitor hybrid system. However, in choosing the capacitance of the supercapacitor, other limitations such as cost and size of the supercapacitor should be considered. A comparison of the gained performance and these limitations is made to find the optimal combination for any tailored application. For such comparison a summary of the percent reduction of the metrics for the LFP and the cost of the hybrid systems are provided in supplementary materials table SM2,3,4.

In applications where size is very crucial such as, cell phones and portable electronics, choosing the smallest supercapacitor that can deliver desired level of performance is chosen. In this case, the targeted supercapacitors are the ones with low capacitances. For example, LFP \Supercapacitor hybrid systems under profile-1 have 20%, 43% and 51% reduction in positive peak currents for 0.5F, 5F and 12F respectively. If 40% decrease in the peak current is enough, a supercapacitor with 5F is the best combination for the LFP under profile-1. Nevertheless, this is also dependent on the applied profile. For instance, in the case of the same LFP/Supercapacitor system but under profile-2 the reduction of the positive peak current is 17%, 50% and 50% for 0.5F, 5F and 12F. As can be seen there is large increase between 0.5F and 5F and no increase at 12F which indicate that supercapacitors with less than 5F are the better choice for hybridization with LFP used under profile-2.

The other limiting factor is the cost of the hybrid system which has great importance while designing any hybrid system. Mass transportation and stationary applications may not have limits in the size of the supercapacitor but the cost is certainly important. If we assume that the cost per kWh of Li-ion battery is 400\$/kWh and supercapacitor is 2500\$/kWh [35,36]; hybridization of LFP with 0.5F will have an increase in the cost by 0.26% while for 200F the increase is 105%. Comparing the increase in the cost percentages with the increase in the performance for each combination in the hybrid systems, we find a linear increase in the cost since it is related to the capacity of the supercapacitors but a nonlinear increase in the performance metrics. For example, under profile-1 the reduction in the positive peak current of the LFP hybridized with 50F is 54% while it is 63% for 200F. However, the increase in the percent cost is 26.4% for the 50F and 105.5% for the 200F. This large increase in the cost is not matched by an increase in the performance which indicates the importance of such analysis in determining the best combination of the battery/supercapacitor hybrid systems.

5. Conclusion

The need to tailor the hybrid systems for high-power-density and high-energy-density applications, with the endless stream of energy storage devices being developed, makes the process of finding the optimal combination by experimental means intractable. The process cannot be guided by a simple investigation of capacities obtained under constant current. A detailed understanding of the current distribution across the hybrid system under widely varying charge/discharge scenarios is needed. This is especially important since the burden-sharing for the battery and the supercapacitor depend on many parameters including the load profile, the history of the devices and the characteristics of the devices itself. For any specific goal regarding how the maximum current, energy, power or charge is going through a specific device, the profile and the devices have to be planned via a thorough investigation of the details. Our simulations are an invaluable tool in order to study different scenarios regarding not only existing but also potential devices that can be hybridized in an unmanaged setting.

Based on the Electrochemical Impedance Spectroscopy of the devices and utilizing Differential Evolution optimization algorithm, current distribution and voltage response of the parallelly connected hybrid battery/supercapacitor systems was predicted with high accuracy. The major advantage of the utilized method is that it is free of any parameterization, fits or subjective inputs. The method was tested for two different Li-ion battery chemistries under three distinct charge/discharge regimes. The modeled results were validated with experimental measurements which showed high accuracy for all systems with less than 2% proportional errors and 1% for most systems. The extension to include simulations of potential combinations with any intended supercapacitor was achieved through the simulation of its Electrochemical Impedance response through equivalent circuit models.

Therefore, the modeling methodology we introduced and verified for hybrid systems can bridge the gap between real life applications of the hybrid systems and the experimental complexities, especially if paired with a data driven approach. In this study we outline the first development of such a method and demonstrate its predictive potential. We envision further studies that focus on the predictive nature of the model to extract exhaustive design rules for applications such as grid scale storage, EVs and consumer electronics.

Author statement

MAZ took all the data and prepared the figures. CBU wrote the code for the analysis, BU conceived the original idea and supervised the project. All authors contributed to the writing of the manuscript.

Declaration of Competing Interest

The authors declare that they have no known competing financial interests or personal relationships that could have appeared to influence the work reported in this paper.

References

- [1] M.R. Lukatskaya, B. Dunn, Y. Gogotsi, Multidimensional materials and device architectures for future hybrid energy storage, *Nature Communications* 7 (1) (2016). Nature Publishing Group, pp. 1–13, 07-Sep-2016.
- [2] P. Simon, Y. Gogotsi, B. Dunn, Where do batteries end and supercapacitors begin? *Science* 343 (6176) (2014) 1210–1211. American Association for the Advancement of Science14-Mar-.
- [3] Y. Liang, H. Dong, D. Aurbach, Y. Yao, Current status and future directions of multivalent metal-ion batteries, *Nature Energy* 5 (9) (2020) 646–656. Nature Research16-Jul-.
- [4] P. Simon, Y. Gogotsi, Perspectives for electrochemical capacitors and related devices, *Nature Materials*, Nature Research (2020) 1–13, 03-Aug-.
- [5] M. Salanne, et al., Efficient storage mechanisms for building better supercapacitors, *Nature Energy* 1 (6) (2016) 1–10. Nature Publishing Group09-May-.

- [6] R.A. Dougal, S. Liu, R.E. White, Power and life extension of battery-ultracapacitor hybrids, *IEEE Transactions on Components and Packaging Technologies* 25 (1) (2002) 120–131.
- [7] J.P. Zheng, T.R. Jow, M.S. Ding, Hybrid power sources for pulsed current applications, *IEEE Transactions on Aerospace and Electronic Systems* 37 (1) (2001) 288–292.
- [8] L. Kouchachvili, W. Yaïci, E. Entchev, Hybrid battery/supercapacitor energy storage system for the electric vehicles, *Journal of Power Sources* 374 (2018) 237–248. November 2017.
- [9] W. Jing, C.H. Lai, W.S.H. Wong, M.L.D. Wong, A comprehensive study of battery-supercapacitor hybrid energy storage system for standalone PV power system in rural electrification, *Applied Energy* 224 (May) (2018) 340–356.
- [10] S. Hajiaghahi, A. Salemnia, M. Hamzeh, Hybrid energy storage system for microgrids applications: A review, *Journal of Energy Storage* 21 (2019) 543–570.
- [11] L. Gao, R.A. Dougal, S. Liu, Active power sharing in hybrid battery/capacitor power sources, Eighteenth Annual IEEE Applied Power Electronics Conference and Exposition, 2003. APEC '03 1 (2003) 497–503.
- [12] L. Gao, R.A. Dougal, S. Liu, Power Enhancement of an Actively Controlled Battery/Ultracapacitor Hybrid, *IEEE Transactions on Power Electronics* 20 (1) (2005) 236–243.
- [13] S. Hajiaghahi, A. Salemnia, M. Hamzeh, Hybrid energy storage system for microgrids applications: A review, *Journal of Energy Storage* 21 (2019) 543–570. August 2018.
- [14] B. Wang, et al., Current technologies and challenges of applying fuel cell hybrid propulsion systems in unmanned aerial vehicles, *Progress in Aerospace Sciences* 116 (2020), 100620. April.
- [15] D. Cericola, P.W. Ruch, R. Kötz, P. Novák, A. Wokaun, Simulation of a supercapacitor/Li-ion battery hybrid for pulsed applications, *Journal of Power Sources* 195 (9) (2010) 2731–2736.
- [16] G. Sikha, B.N. Popov, Performance optimization of a battery-capacitor hybrid system, *Journal of Power Sources* 134 (1) (2004) 130–138.
- [17] R. Chandrasekaran, G. Sikha, B.N. Popov, Capacity fade analysis of a battery/supercapacitor hybrid and a battery under pulse loads - Full cell studies, *Journal of Applied Electrochemistry* 35 (10) (2005) 1005–1013.
- [18] E. Özdemir, C.B. Uzundal, B. Ulgut, Zero-Free-Parameter Modeling Approach to Predict the Voltage of Batteries of Different Chemistries and Supercapacitors under Arbitrary Load, *Journal of The Electrochemical Society* 164 (6) (2017) A1274–A1280.
- [19] Y. Wang, X. Lin, Q. Xie, N. Chang, and M. Pedram, “Minimizing state-of-health degradation in hybrid electrical energy storage systems with arbitrary source and load profiles,” 2014, pp. 1–4.
- [20] A. Ostadi, M. Kazerani, A Comparative Analysis of Optimal Sizing of Battery-Only, Ultracapacitor-Only, and Battery-Ultracapacitor Hybrid Energy Storage Systems for a City Bus, *IEEE Transactions on Vehicular Technology* 64 (10) (2015) 4449–4460.
- [21] “A reference book of driving cycles for use in the measurement of road vehicle emissions | TRL.”.
- [22] G. Sikha, R.E. White, B.N. Popov, A Mathematical Model for a Lithium-Ion Battery/Electrochemical Capacitor Hybrid System, *Journal of The Electrochemical Society* 152 (8) (2005) A1682.
- [23] A. Seaman, T.-S. Dao, J. McPhee, A survey of mathematics-based equivalent-circuit and electrochemical battery models for hybrid and electric vehicle simulation, *Journal of Power Sources* 256 (2014) 410–423.
- [24] C. Zou, L. Zhang, X. Hu, Z. Wang, T. Wik, M. Pecht, A review of fractional-order techniques applied to lithium-ion batteries, lead-acid batteries, and supercapacitors, *Journal of Power Sources* 390 (2018) 286–296.
- [25] B. Ulgut, C.B. Uzundal, E. Özdemir, Analysis of Errors in Zero-Free-Parameter Modeling Approach to Predict the Voltage of Electrochemical Energy Storage Systems under Arbitrary Load, *ECS Transactions* 77 (11) (2017) 99–104.
- [26] M.A. Zabara, B. Ulgut, Electrochemical Impedance Spectroscopy based voltage modeling of lithium Thionyl Chloride (Li/SOCl₂) primary battery at arbitrary discharge, *Electrochimica Acta* 334 (2020), 135584.
- [27] R. Storn, K. Price, Differential Evolution - A Simple and Efficient Heuristic for Global Optimization over Continuous Spaces, *Journal of Global Optimization* 11 (4) (1997) 341–359.
- [28] M. Weiss, P. Bonnel, R. Hummel, A. Provenza, U. Manfredi, On-road emissions of light-duty vehicles in Europe, *Environmental Science and Technology* 45 (19) (2011) 8575–8581.
- [29] J. Bisquert, Influence of the boundaries in the impedance of porous film electrodes, *Physical Chemistry Chemical Physics* 2 (18) (2000) 4185–4192.
- [30] P. Virtanen, et al., SciPy 1.0: fundamental algorithms for scientific computing in Python, *Nature Methods* 17 (3) (2020) 261–272.
- [31] “nidaqmx • PyPI.” [Online]. Available: <https://pypi.org/project/nidaqmx/>. [Accessed: 27-Dec-2020].
- [32] B. Ulgut, C.B. Uzundal, E. Özdemir, Analysis of errors in zero-free-parameter modeling approach to predict the voltage of electrochemical energy storage systems under arbitrary load, *ECS Transactions* 77 (11) (2017) 99–104.
- [33] M.R. Palacín, A. De Guibert, Batteries: Why do batteries fail? *Science* 351 (6273) (2016) 1253292. American Association for the Advancement of Science 05-Feb-.
- [34] J. Vetter, et al., Ageing mechanisms in lithium-ion batteries, *Journal of Power Sources* 147 (1–2) (2005) 269–281.
- [35] P.K.S. Roy, H.B. Karayaka, Y. Yan, Y. Alqudah, Size optimization of battery-supercapacitor hybrid energy storage system for 1MW grid connected PV array, 2017 North American Power Symposium, NAPS (2017) 2017.
- [36] P.K.S. Roy, H.B. Karayaka, Y. Yan, Y. Alqudah, Investigations into best cost battery-supercapacitor hybrid energy storage system for a utility scale PV array, *Journal of Energy Storage* 22 (2019) 50–59. July 2018.